N72-23795

PREDICTION OF THE EFFECTS OF THERMAL STRATIFICATION ON PRESSURE AND TEMPERATURE RESPONSE OF THE APOLLO SUPERCRITICAL OXYGEN TANK

I. M. Chen and R. E. Anderson

North American Rockwell Corporation
Space Division, Downey, California

A semi-empirical design-oriented model has been developed for the prediction of the effects of thermal stratification on tank pressure and heater temperature response for the Apollo supercritical oxygen tank. The heat transfer formulation describes laminar free convection at low-g and takes into account the radiation and conduction processes occurring in the tank. The non-equilibrium thermodynamic behavior of the system due to localized heating of the stored fluid is represented by the characteristics of a discrete number of fluid regions and thermal nodes. Solutions to the time dependent variable fluid property problem are obtained through the use of a reference temperature procedure. A criterion which establishes the reference temperature as a function of the fluid density ratio, ρ/ρ_{cr} is derived. The analytical results are compared with the flight data.

I. Introduction

As a result of the use of supercritical cryogenic systems for space missions, considerable interest has been directed to the phenomenon of thermal stratification at low-gravity and its effects on the storage and expulsion performance of the system. The need for a better understanding of the problem is further emphasized due to the design support requirements for the present configuration of the Apollo cryogenic oxygen storage system (CSS). Of basic concern to the CSS is the degree of stratification due to local heating of the stored medium by the tank heating element. The effects on the heater temperature and the tank pressure response, and potential pressure decay, are expected to be significantly accentuated by the extremely low acceleration flight environment.

In view of the difficulty associated with obtaining analytic solutions to the non-equilibrium thermodynamic phenomenon for a geometrically complex system, a semi-empirical approach, based on subdividing the system into an arbitrary number of regions and thermal nodes, was selected for modeling the system.

The model was correlated initially with experimental data derived from a series of one-g, heat transfer tests. Owing to the exact geometric similarity of the test article to the flight hardware, these tests provided basic characteristic data and system constants essential for determining the radiative and conductive transport properties of the system. Free convective heat transfer characteristics of the CSS heater in low Rayleigh number regime were investigated through scaling tests. The results served as a basis for checking the adequacy of the model.

Using the refined model, pre-flight prediction of the Apollo 14 CSS performance was generated. Results showed good agreement with the flight data, especially in the low fluid density range. Post-flight data analysis provided a broad spectrum of system information for further model correlation and refinement.

Of significance in the model verification is the correlation of the free convection heat transfer process in the supercritical temperature region where the fluid properties exhibit the most severe variations. A simple solution to the variable fluid property problem was obtained through the use of a reference temperature procedure.

To provide perspective on the capabilities of the simulation model, computer results were compared with Apollo 14 flight data over a range of fluid densities, acceleration, and heater input power levels.

II. Description of the Model

The model of the Apollo cryogenic oxygen storage system was formulated on the basis of its design configuration and flight operational characteristics. The model describes the laminar free convection at low-gravity and takes into account the radiation and conduction phenomena occurring in the tank. The non-equilibrium thermodynamic behavior of the system due to localized heating of the stored fluid in a low acceleration environment is represented by three arbitrary cells as shown in Figure 1. The acceleration vector due to the rotation of the spacecraft is assumed to be normal to the heater axis. The first cell is formed by the accumulation of the rising boundary layer flow generated by the thermal energy released from the external surface of the heater. The growth of this (external) cell is governed by the rate at which the boundary layer flow is developed. The second cell is formed within the hollow structure of the heating element. The relatively confined fluid in this cell expands and contracts as its temperature fluctuates. The change of the fluid density in this(internal) cell causes part of the fluid mass to flow in or out of this region. The third cell comprises the main (bulk) region which slowly gains in temperature responding to heat transfer from the tank shell and the associated tank internal structures.

Specific system hardware included in the model are the heater, fluid quantity probe, and the attendent tank shell structures. The thermal capacitance effects of these components are lumped by using a discrete number of thermal nodes. The paths by which energy is transported and the interrelationships of the nodal masses or the fluid cells are depicted in Figure 2. The thermal energy generated from the electrical heater is transmitted predominantly by radiation and conduction to the hardware components and by convection to the external and internal cell fluids. The radiant energy absorbed by the shell structure is transmitted, in turn, through convection to the bulk cell fluid. The heat and mass transport process between the three cells are evaluated by the total enthalpies associated with the fluid flows crossing the cell boundaries. Since the kinetic energy associated with the free laminar boundary layer flow is rather small in the low-g field, the convective transport of momentum from the external cell to the bulk cell is considered to be insignificant. Heat transfer due to

fluid mixing effects and cell temperature gradient is estimated by an idealized conduction analogy for a stable thermal layer with an arbitrary cell interface.

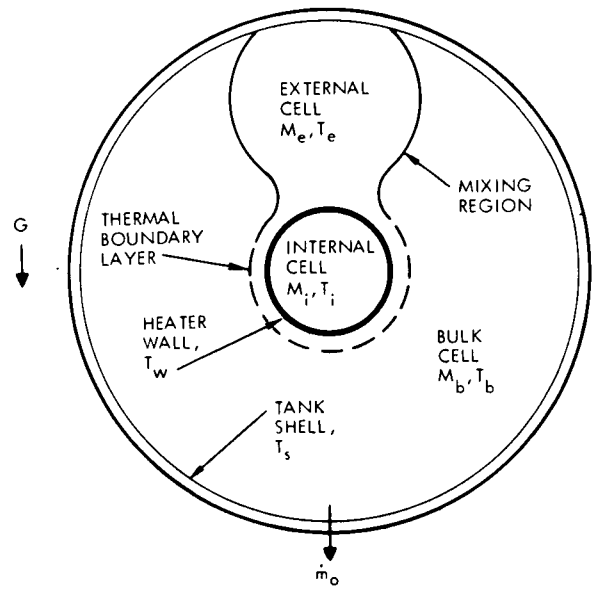

Fig. 1 Analytical Model

Test data derived from a series of one-g scaling tests were used to establish the basic system characteristics related to heat transfer. In order to evaluate the constants appearing in the analysis, radiative and conductive heat fluxes were measured with an actual full scale evacuated tank in which the surface emission and reflective characteristics, and the geometry of the tank components were duplicated. Data related to the convective heat transfer process at low-g was obtained from experiments using oxygen at reduced pressure as the test fluid based on Rayleigh number scaling techniques. Due to the inherent limitations associated with scaling and selection of a fluid with suitable thermal physical properties, only a limited Rayleigh number regime, encompassing a few equivalent acceleration levels and fluid density data points, was evaluated.

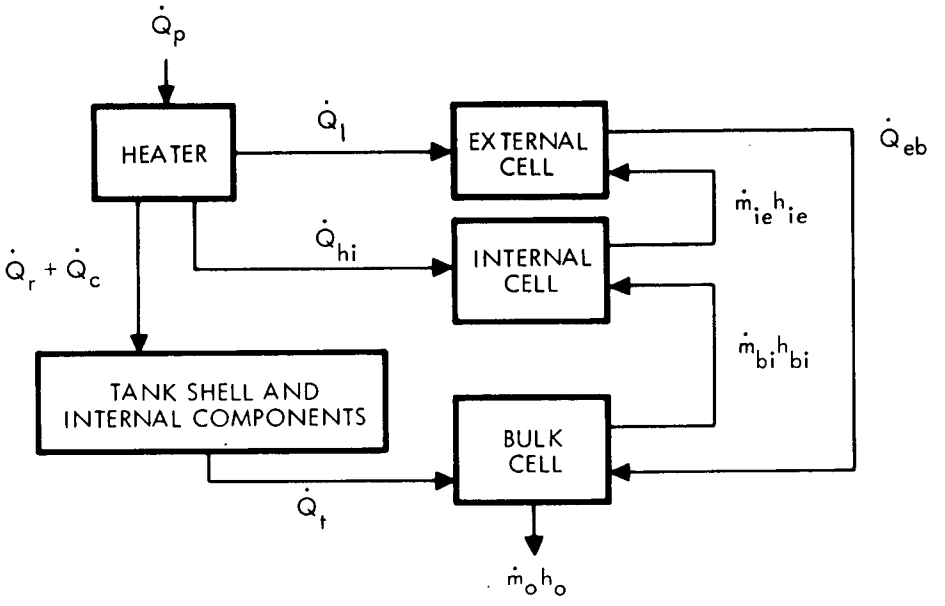

Fig. 2 Model Energy Flow Diagram

In the following sections, the equations essential to the description of the heat transfer and thermodynamic characteristics of each of the three lumped cells will be presented and the coupling of the equations to form the system dynamic simulation model will be discussed.

III. System Equations

Heat Transfer Formulation

The description of the thermal radiation and conductive processes between the various nodal masses assumed for the model are based on Stefan-Boltzmann and Fourier law equations. The net radiant energy interchange rates between interaction surfaces of the heater and the tank internal components are expressed as

$$q_{r,net} = \sum_{k=1}^{m} \sigma \mathcal{F}_{w,k} (T_w^4 - T_k^4) \qquad (1)$$

where $\mathcal{F}_{w,k}$ is the node-to-node interchange factor, the values of which, for the CSS, were established by experiments.

The conductive flux at a nodal point is represented by

$$q_{c,j} = \sum_{j=1}^{n} \frac{k_j}{x_j} (T_w - T_j) \tag{2}$$

where k_j is the effective thermal conductance and x_j is the penetration thickness.

The formulation, describing the convective energy transport process from the heater to the external, internal, and bulk cells, is separately summarized as follows.

External Cell. The heat energy transferred to the fluid external to the heater is assumed to be absorbed completely by the boundary layer which forms a part of the external cell. The temperature of the external cell fluid is assumed to be uniform; as the rising boundary flow is added to the cell, it is assumed to mix instantaneously with all of the external cell fluid. Detailed analysis of the free laminar boundary layer heat transfer has been extensively treated in the literature (References 1, 2, 3).

Estimates of the heat transfer rates from the horizontal cylindrical heater surface are derived from a basic vertical flat plate analogy which gives the result that heat transfer from a vertical flat plate and a horizontal circular cylinder are identical when the height of the plate is 2.5 times the cylinder diameter.

The integral forms of the momentum and energy equations for steady state boundary layer flow on a vertical flat plate are:

$$\frac{d}{dX} \int_o^\delta u^2 dy = g\beta \int_o^\delta (T - T_b)\, dy - \nu \left[\frac{du}{dy}\right]_w \tag{3}$$

$$\frac{d}{dX} \int_o^\delta u\,(T - T_b)\, dy = \frac{-k}{\rho c_p} \left[\frac{dT}{dy}\right]_w \tag{4}$$

Using the conventional approximations for the velocity and temperature profiles for the boundary layer flow, Eqs. (3) and (4) can be reduced into a set of simultaneous ordinary differential equations, the solution of which leads to the determination of $\delta(x)$ and $u(x)$, (Reference 3).

A dimensionless representation of the boundary layer heat transfer, the local Nusselt number, is then obtained by relating the local heat transfer coefficient to the boundary layer thickness and thermal conductivity.

$$Nu_x = \frac{h_x x}{k} = \frac{q}{(T_w - T_b)} \frac{x}{k} = 2\left(\frac{x}{\delta}\right) \qquad (5)$$

The average heat flux for a vertical flat plate based upon the integrated local heat transfer coefficient can be expressed as

$$\bar{q} = \frac{8}{3} \frac{k}{\delta} (T_w - T_b) \qquad (6)$$

The average convective heat flux for the horizontal cylindrical heater is estimated based on the average heat flux computed for a flat plate, Eq. (6), with an equivalent characteristic dimensional height (Reference 3).

The growth of the external cell reflecting the increase of its mass, m_e, is determined by integrating the boundary layer flow.

$$m_e = \int_0^t \dot{m}_\ell \, dt \qquad (7)$$

where

$$\dot{m}_\ell = \rho \, \bar{v}(x,t) \, \delta(x,t) \, L \qquad (8)$$

The variables ρ, $\bar{v}$, and δ are respectively the instantaneous fluid density, mean boundary layer velocity, and thickness of the boundary layer flow when it mixes with the external cell fluids, i.e., at the top of the equivalent plate.

The shape of the external cell is arbitrary. The transfer of energy at the hypothetical cell boundary to the bulk fluids due to mixing in this model is approximated by the Fourier conduction law equations with an arbitrary scale length.

Internal Cell. The estimates of heat transfer from the interior surface of the heater to the cell fluid in an enclosed space is complicated and empirical results must also be used. Theoretical analyses dealing with laminar steady convective flows and heat transfer specifically for a horizontal tube with circular cross-section have been examined by Martini and Churchill (Reference 4) and Weinberg (Reference 5). Solutions of partial differential equations describing the conservation of mass and energy for the system have yielded reasonable predictions of temperature fields for specific cases of interest. These results are in good agreement with experimental measurements. Estimates of the average heat transfer coefficient for free convection inside a horizontal cylinder can generally be obtained using the following correlation, (Reference 6)

$$\frac{\overline{Nu}}{Gr^{1/4}} = c_1 \left[\frac{Pr^2}{1+Pr}\right]^{1/4} \tag{9}$$

For the ranges of Prandtl and Grashof numbers considered for the internal cell, $c_1 = 0.35$ is assumed.

To account for the effects of the expansion and contraction of the internal cell fluid as its temperature fluctuates during a heating cycle, the change of the fluid mass in the internal cell is given by

$$\dot{m}_i = V_i \dot{\rho}_i \tag{10}$$

where V_i is the internal physical volume of the heater tube and the rate of change in the cell fluid density is

$$\dot{\rho}_i = -\left|\beta \rho \dot{T}\right|_i \tag{11}$$

The fluid mass expelled due to the internal cell temperature rise ($\dot{T}_i$ is positive) is assumed to be mixed with the external cell. Since the enthalpy of the expelled fluid element greatly exceeds its kinetic energy, the momentum transfer is neglected. For the case where the cell temperature decreases ($\dot{T}_i$ is negative), the fluid from the bulk region is assumed to be drawn into the internal cell compensating for the fluid density change.

Bulk Cell. It is assumed that the temperature of the bulk cell is uniform but varies with time. During a heater cycle, the tank shell temperature increases due to radiative and conductive heat flux from the heater. The convective heat transfer, due to the temperature gradient developed between the tank shell and the bulk fluid, contributes to the bulk fluid temperature rise.

The laminar free convective heat transfer from the spherical tank shell to the bulk fluid is approximated by a dimensionless heat transfer parameter correlation, similar to that used for the cylindrical internal cell.

$$\frac{\overline{Nu}}{Gr^{1/4}} = c_2 \left[\frac{Pr^2}{1+Pr}\right]^{1/4} \tag{12}$$

On the basis of scaling test data correlation, $c_2 = 0.45$ is assumed.

The effective heat transfer surface area for the tank shell is estimated on the basis of the geometric volume equivalence of a cylindrical container.

Thermodynamic Formulation

The development of the equation describing the thermodynamic behavior of the supercritical cryogenic storage system is based on the statement of the First Law. Each cell of the model is assumed to be a totally enclosed thermodynamic system with arbitrary moving boundaries. Letting Q be the total heat input in the system, the basic equation relating the total internal energy and thermodynamic variables of the system is

$$dU = \sum_{j=1}^{n} h_j dm_j + dQ - pdV \tag{13}$$

where h_j represents the specific enthalpies associated with the masses, m_j, added and/or removed from the system.

Treating p and ρ as the independent thermodynamic state variables, Eq. (13) may be expressed as

$$\rho V \left[\left(\frac{\partial u}{\partial p} \right)_\rho dp + \left(\frac{\partial u}{\partial \rho} \right)_p d\rho \right] + u d(\rho V) =$$

$$\sum_{j=1}^{n} h_j dm_j + dQ - pdV \qquad (14)$$

By letting

$$\phi = \frac{1}{\rho} \left(\frac{\partial p}{\partial u} \right)_\rho$$

and

$$\psi = \rho \left(\frac{\partial u}{\partial \rho} \right)_p$$

and treating the system variables as functions of time, the above equation for an adiabatic cell can be transformed to a characteristic equation relating the cell volume, V, to the system pressure, p, as

$$\frac{dV}{dp} = \frac{1}{(\rho\psi - p)} \left\{ \frac{V}{\phi} - \left[\sum_{j=1}^{n} h_j \dot{m}_j - (u + \psi) \dot{m} \right] \frac{1}{\dot{p}} \right\} \qquad (15)$$

Let η be the energy rate parameter representing the sum of the heat and mass rates of addition or removal from the cell. Then,

$$\frac{dV}{dp} = \frac{1}{(\rho\psi - p)} \left[\frac{V}{\phi} - \frac{\eta - (u + \psi)\dot{m}}{\dot{p}} \right] \qquad (16)$$

where

$$\eta = \sum_{j=1}^{n} h_j \dot{m}_j$$

It is convenient to define additional parameters as

$$\Omega = \frac{\eta - (u + \psi)\,\dot{m}}{(\rho\psi - p)}$$

and

$$\Gamma = \frac{V}{\phi\,(\rho\psi - p)}$$

Eq. (16) for the three cells can be rewritten in a generalized form as

$$\left(\frac{dV}{dp}\right)_j = \Gamma_j - \frac{\Omega_j}{\dot{p}} \qquad (17)$$

Based upon the assumptions made relating the heat and mass transfer across the specific cell boundaries, the energy rate parameters, η_e, η_i, and η_b, for the external, internal, and bulk cells, respectively, are expressed as follows.

First,

$$\eta_e = h_\ell \dot{m}_\ell + h_i \dot{m}_i - \dot{Q}_{eb}$$

The first two terms on the right hand side of the equation represent the enthalpies associated with the boundary layer flow generated by the external surface of the heater and that associated with the flow expelled from the internal cell during the heat up process. Q_{eb} is the interfacial heat transfer rate from the external to bulk cell.

Similarly,

$$\eta_i = h_b \dot{m}_b - h_i \dot{m}_i + \dot{Q}_{hi}$$

The first two terms on the right hand side of the equation represent the enthalpies associated with flow replenished from the bulk cell during cooling and the flow expelled from the internal cell during heating of the cell fluid. $\dot{Q}_{hi}$ is the heat transfer rate from the heater interior surface to the internal cell.

And finally,

$$\eta_b = \dot{Q}_{eb} + \dot{Q}_b - h_b \dot{m}_t$$

where $\dot{Q}_b$ is the sum of all radiative and convective heat transfer rate from the tank shell and interior components, and $\dot{m}_t$ is the mass flow rate transferred from the bulk cell to the adjacent cells and includes that which is withdrawn from the tank.

Coupling of the Cells

Based upon the cell volume relationships, the total tank internal volume, V_t, may be expressed as

$$V_t = V_e + V_i + V_b \tag{18}$$

By differentiating Eq. (18) with respect to the tank pressure, assuming the tank to be elastic, and letting

$$\frac{dV_t}{dp} = \epsilon \tag{19}$$

an expression which establishes the dynamic coupling effects of the individual cells is obtained.

$$\frac{dV_e}{dp} + \frac{dV_i}{dp} + \frac{dV_b}{dp} = \epsilon \tag{20}$$

Replacing the three derivative terms in Eq. (20) by the respective characteristic equation defined in Eq. (17) and solving the resulting equation in terms of $\dot{p}$, one obtains

$$\dot{p} = \frac{\sum_{j=1}^{3} \Omega_j}{\sum_{j=1}^{3} \Gamma_j - \epsilon} \tag{21}$$

In this equation, the index, j = 1,2,3, designates the parameters for the external, internal, and bulk cells, respectively.

Eq. (21) can be integrated to obtain the tank pressure as a function of time reflecting the non-equilibrium thermodynamic effects of the transient heat and mass transfer processes occurring during a heating and expulsion cycle of a single phase supercritical cryogenic tank.

Pressure Decay Potential

The non-equilibrium thermodynamic state in the tank is inherently unstable. Any external perturbation will cause the tank pressure to decay because of the natural tendency of the system to establish thermal equilibrium. The pressure decay potential of such a system may be computed by an approximate heat deficiency equation based on the difference between the average heat content of the system and that of the sum of the stratified cells. The equation is

$$\Delta Q = (\bar{\rho}\bar{u})\, V - \sum_{j=1}^{3} (\rho u V)_j \tag{22}$$

where ΔQ stands for heat deficiency, the bar denotes average parameter values, and the summation is extended over the three cells into which the thermodynamic system has been subdivided.

The instantaneous pressure decay potential can then be determined by

$$\Delta p_{max} = \frac{\bar{\phi}}{V} \Delta Q$$

Using ΔQ defined in Eq. (20) and taking into account the elastic effects of the tank, the maximum pressure collapse potential of the stratified system can be expressed as:

$$\Delta P_{max} = \frac{\bar{\phi}(\bar{\rho}\bar{u})V - \sum_{j=1}^{3}(\rho u V)_j}{V - \epsilon\,\bar{\phi}\bar{\rho}\bar{\theta}} \tag{23}$$

The pressure dependencies of u, θ, and ϕ are considered and evaluated by solving the above equation through an iterative procedure.

IV. Comparison of Analytical and Flight Data

Numerical solutions to the time dependent model equations were obtained in terms of heater temperature and tank pressure for a wide range of parametric system conditions. Major system and operational parameters considered in the study include heater input power, local acceleration level, and fluid expulsion flow rate. In the following sections, significant results and observations which are critical to the system design evaluation and flight performance predictions are discussed. Comparisons of these results with Apollo 14 flight data are presented.

Peak Heater Temperature

During an expulsion process, the supercritical tank pressure is maintained within a prescribed band by controlling the heater input power through a pressure switch. In the course of a tank pressure cycle and at a given heater input power level, the heater temperature reaches its maximum value either when the tank pressure reaches the maximum pressure switch setting and the heater power is cut off, or when the thermal equilibrium is approached and the heater is saturated. The peak temperature and its variability due to bulk fluid density change is of particular concern to the system designers.

Predicted values of peak heater temperatures plotted as a function of bulk density showing its dependencies on local acceleration level and heater input power are illustrated in Figures 3 and 4, respectively. The dominance of convective heat transfer in the high density region ($\rho > 50$ lb/cu ft) is evidenced by the fact that the heater

saturates at relatively low temperatures (approximately -150°F). The average heat transfer coefficient is of the order of 5 Btu/hr-sq ft-R. The peak heater temperature exhibits a weak dependence on gravity. A temperature difference of approximately 20 degrees is observed as the local acceleration level changes by two orders of magnitude.

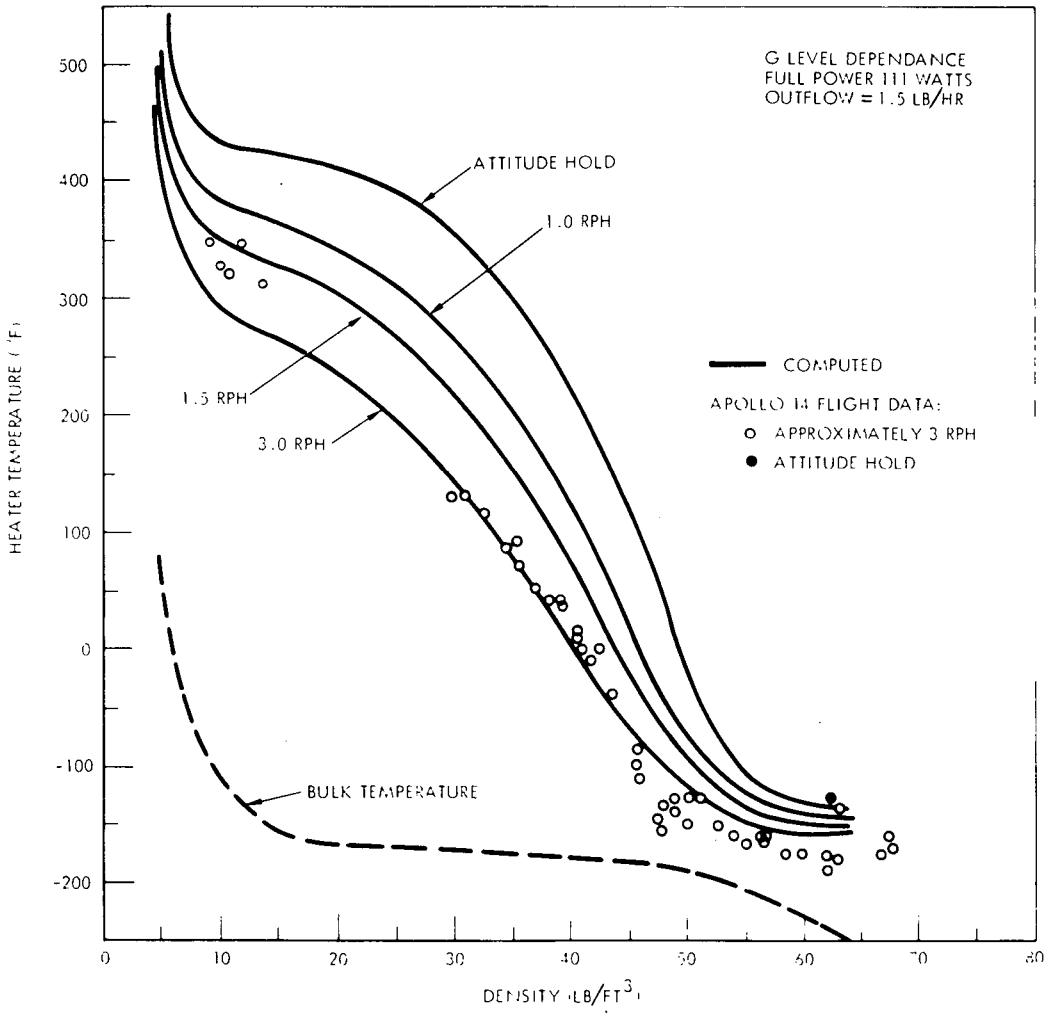

Fig. 3 Peak Heater Temperature Vs. Fluid Bulk Density for Selected Acceleration Levels

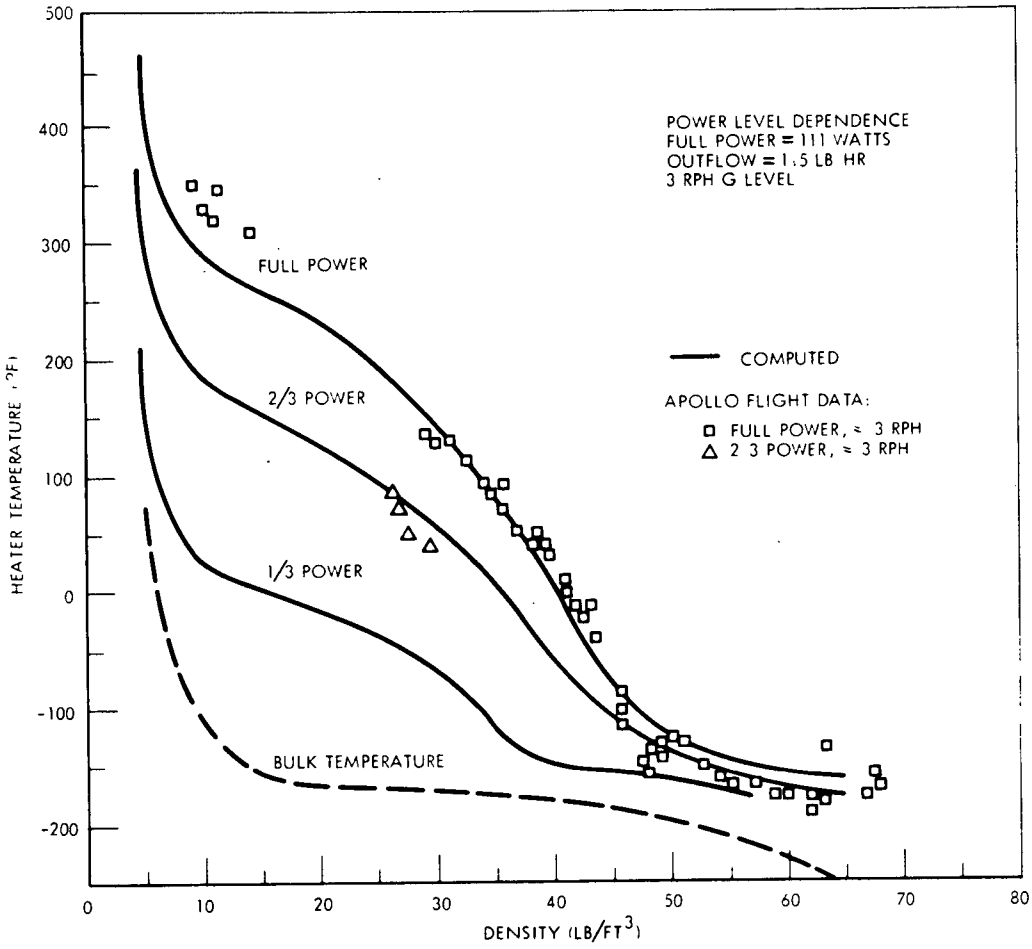

Fig. 4 Peak Heater Temperature Vs. Fluid Bulk Density for Selected Heater Input Power Levels

In the intermediate density range ($10 < \rho < 50$ lb/cu ft), the influence of g-level on the peak heater temperature is pronounced. The temperature shows a wide divergence as the fluid density decreases. For the g-level limits shown in the graph, as much as 200 degrees temperature difference exists over most of the density range.

At densities below 10 lb/cu ft, the peak heater temperatures at the noted g condition begin to converge showing the sharply reduced convective heat transfer rate. The average heat transfer coefficient in this range is approximately 0.5 Btu/hr-sq ft-R. Below a bulk density of 5 lb/cu ft, the heater temperature saturates, as the radiation mode of heat transfer becomes dominant, and shows insignificant g dependencies.

The heater input power has a marked influence on the peak heater temperature when the tank fluid density drops below 45 lb/cu ft as shown in Figure 4. At a constant expulsion rate and g level, the reduction of heater input power has a gradually more pronounced effect on lowering the peak heater temperature as the fluid density decreases. The magnitude of the peak temperature reduction reflects the lower heater temperature response rates at lower input power level while the convective heat transfer rates remain relatively constant. In view of this characteristic behavior, heater power management in the lower density range appears to be an effective means for constraining the peak heater temperature within allowable limits. However, it should be noted that there is a minimum heater power that must be provided to maintain tank pressurization for a given expulsion flow rate.

Heat Transfer Near the Critical Temperature

The comparison of analytical and flight data in the critical region, i.e., pressure greater than the critical pressure and temperature in the region of the critical temperature, affirmed that the convective heat transfer rate differs significantly from that in other thermodynamic regions. This is evidenced by the fact that dramatically lower peak heater temperatures were observed when the bulk fluid density was greater than 48 lb/cu ft. This apparent increase in heat transfer near the critical temperature regime resulting in lower heater temperature is attributed to the abrupt changes in the fluid thermal transport properties (Reference 7). Early studies showed that conventional methods for correlating the convective heat transfer data were unable to account for the effects exhibited by supercritical fluids in this temperature region (References 8 and 9). For supercritical fluids, some investigations have been performed to evaluate the heat transfer in the forced convection regime. However, there is a lack of experimental work related to the free laminar convection region, especially at low Rayleigh numbers. A method which has been applied with reasonable success in correlating heat transfer data in the critical temperature regime involves the use of a well established variable fluid property scheme. Extending this procedure to the present analysis, a variable reference temperature method, similar to that suggested by Eckert (Reference 10) was chosen. In this method, fluid properties are evaluated at a reference temperature, T_{ref}, where $T_{ref} = T_w - \alpha(T_w - T_b)$. The dimensionless parameter, α, is assumed to be a unique function of ρ_b/ρ_{cr}, where ρ_{cr} is the fluid density at the critical temperature. Based upon the Apollo 14 flight data, a criterion relating the dimensionless temperature ratio, $(T_w - T_{ref})/(T_w - T_b)$, to the density ratio, ρ_b/ρ_{cr} was established as shown in Figure 5.

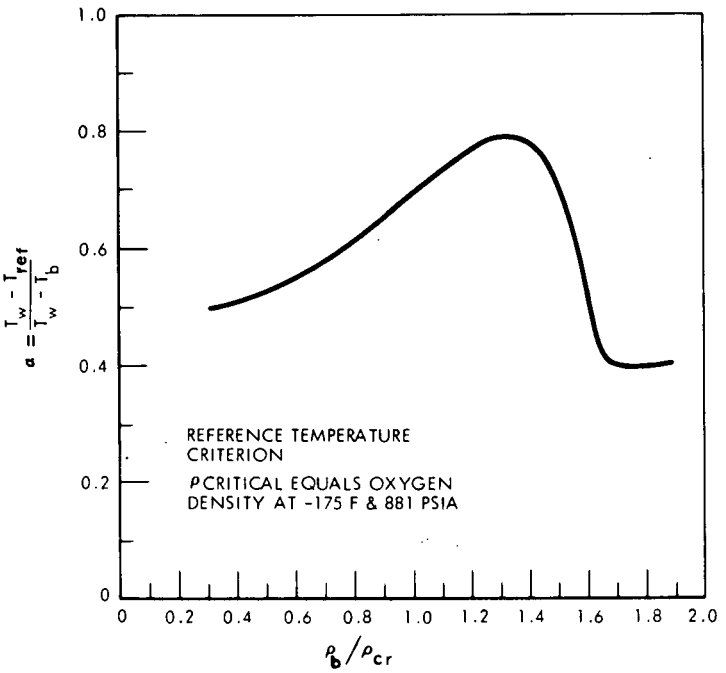

Fig. 5 Dimensionless Temperature Ratio Vs. Critical Density Ratio

Tank Pressure Response

The pressure rise and decay times associated with a heater cycle (pressure cycle period) are affected by the expulsion flow rate at a given heater input power level and fluid density. The pressure cycle frequency as a function of bulk fluid density is shown in Figure 6 for a range of expulsion flow rate conditions. In the high fluid density region, ($\rho > 55$ lb/cu ft), the expulsion flow rate has the greatest influence on the cycle frequency. In this region, the cycle frequency for a given flow rate is nearly constant. As the density is decreased, the cycle frequency is sharply reduced because of the rapid changes of the fluid thermal transport properties and resultant reduction in convective heat transfer rates. In addition, the characteristic variation in the thermodynamic function θ also contributes to the characteristic shift in frequency. It is of interest to note that the pressure cycle frequency becomes less sensitive to flow rate variability at lower fluid densities.

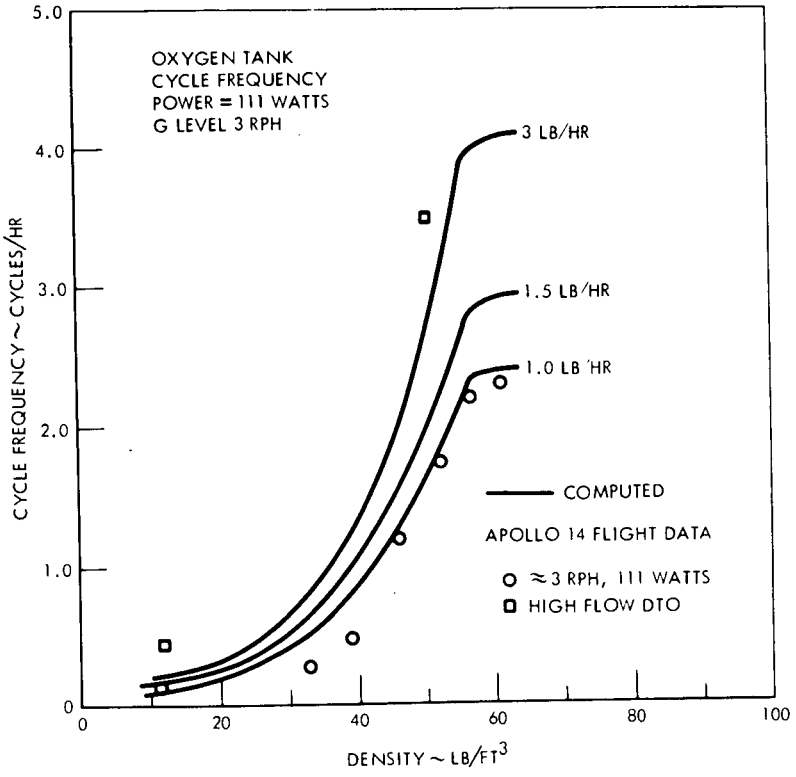

Fig. 6 Tank Pressure Cycle Frequency Vs. Fluid Bulk Density for Selected Expulsion Rates

Flight Data Correlation

Figures 7 and 8 compare the analytical predicted heater temperature and pressure response at two selected bulk fluid density conditions with the Apollo 14 flight data. The flight and analytical values of the peak heater temperature and the pressure rise rate are found to be in good agreement. The model shows a slightly higher initial heater temperature response rate. This is partially due to the quasi-steady state approximation of the heat transfer transients and the inaccuracies associated with the lumped parameter approach used for the model.

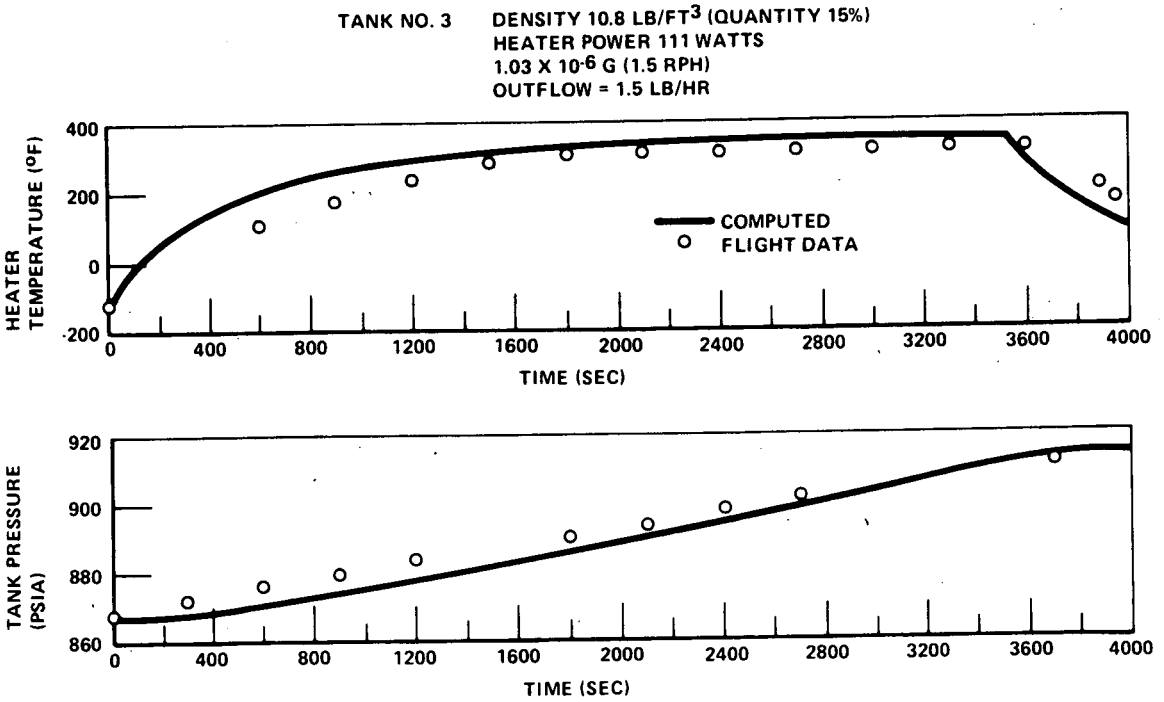

Fig. 7 Heater Temperature and Tank Pressure Vs. Time at O_2 Quantity 15%

Figure 9 compares the model predictions with the flight data for a case at relatively high bulk density conditions and high expulsion flow rate. The system characteristics associated with repeated cycling of the heater are illustrated. The comparison of the temperature and pressure response data showed close agreement for the initial cycles. The slight deviation that appears for the remaining cycles is due to changes in outflow and g-level occurring in flight which are not accounted for in the simulation. It is of interest to note that there is only a small net heater temperature gain (0.5 degrees) after each successive heater cycle.

Figure 10 shows the time characteristic changes in the temperatures of the three hypothetical cells of the model. The accumulative increase in the magnitude of the maximum pressure decay potential reflecting the progressively increased degree of stratification in the system is also illustrated. Among the three cells, the most significant gain in fluid temperature is noted in the internal cell due to the lack of cooling during the heater-off periods. This phenomenon contributes appreciably to the rise of the maximum decay potential. To minimize the problems associated with the potential tank pressure collapse, particularly at high fluid bulk density conditions, a passive means which can facilitate cooling of the internal cell fluids would be highly effective.

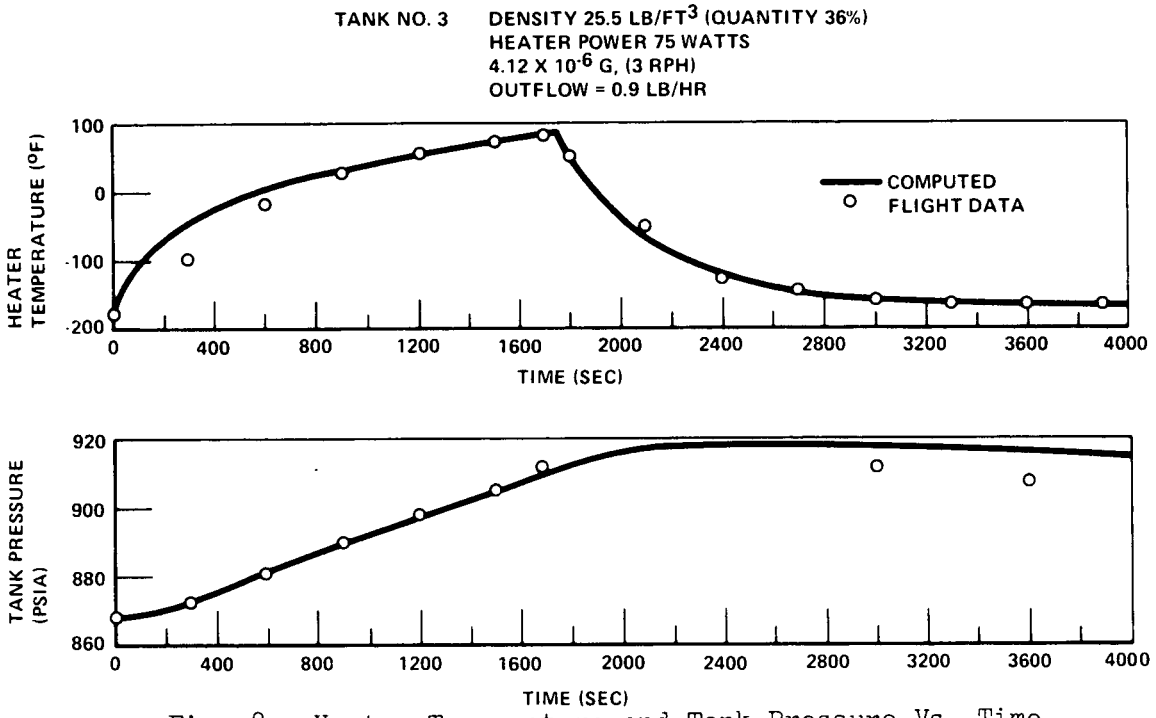

Fig. 8 Heater Temperature and Tank Pressure Vs. Time at O_2 Quantity 36%

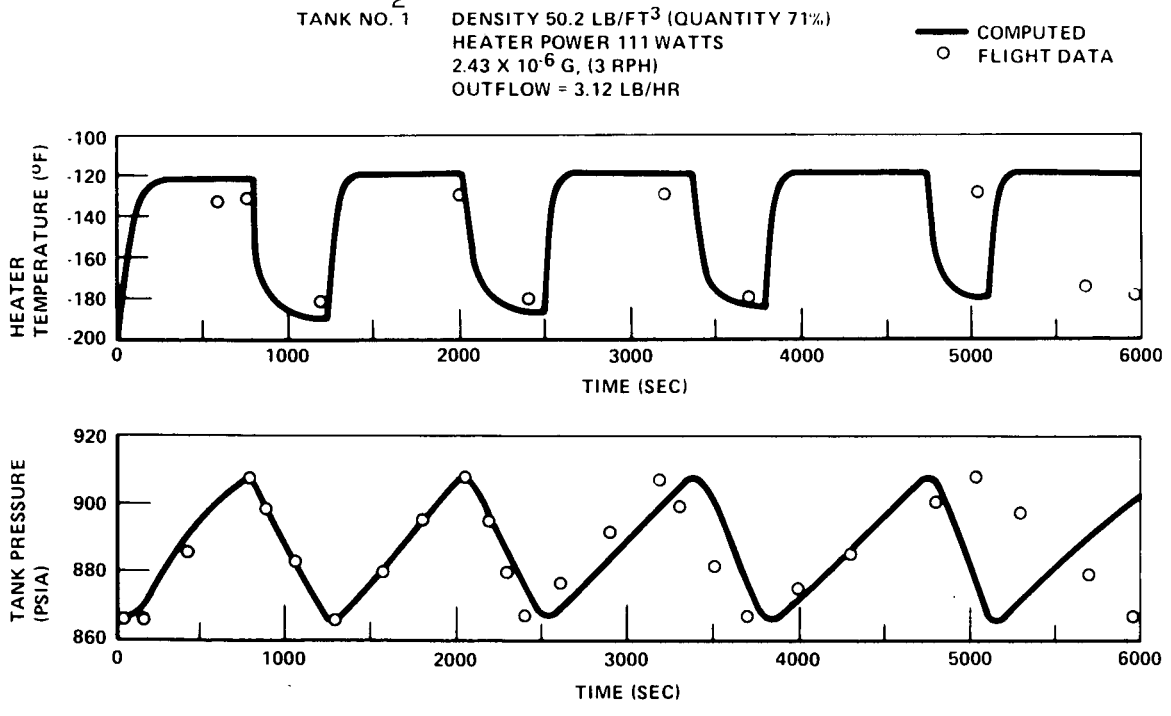

Fig. 9 Heater Temperature and Tank Pressure Vs. Time at O_2 Quantity 71%

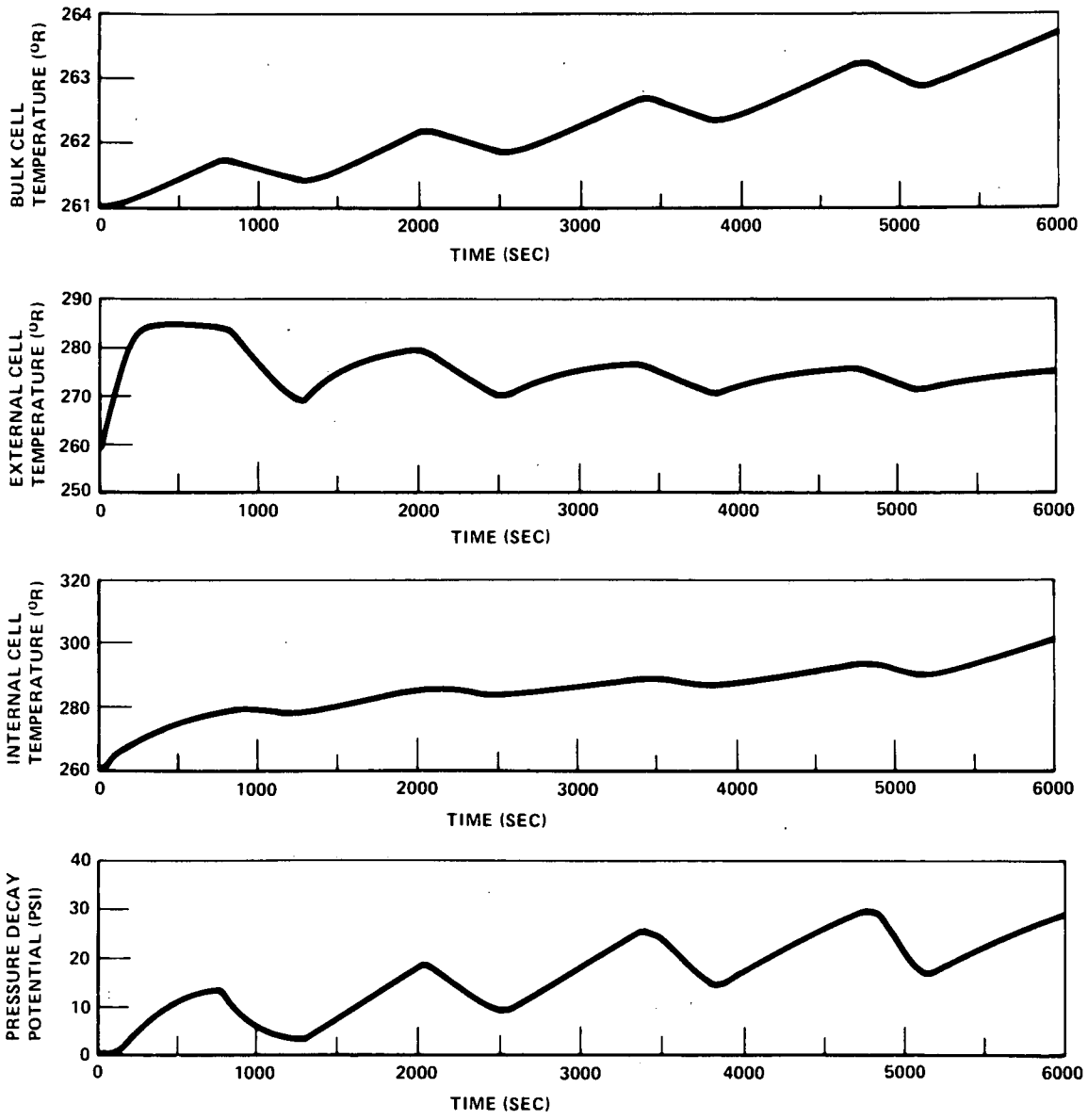

Fig. 10 Fluid Cell Temperature and Pressure Decay Potential Vs. Time at O_2 Quantity 71%

V. Concluding Remarks

Although the Apollo 14 flight data provided a limited number of applicable measurement points pertaining to the CSS, development of the analytical model and correlation of available data have provided insight and understanding of the low-g free convective heat transfer and non-equilibrium behavior of the supercritical cryogenic storage system. On the basis of the analysis of the flight data and parametric evaluation results of the model, the following concluding remarks are presented.

1. When the mean boundary layer temperature is near the critical temperature regime, the heater saturates at relatively low temperatures due to significantly high convective heat transfer associated with large fluid thermal transport property changes. The peak heater temperature shows a noticeable dependence on the magnitude of the heater input power and is influenced to a lesser degree by the acceleration level.

2. When the fluid bulk density drops below 10 lb/cu ft, the convective heat transfer rate is sharply reduced. At a bulk density below 5 lb/cu ft, the radiation mode of heat transfer becomes dominant. The heater temperature then saturates as the radiative heat transfer rate approaches an asymptotic level for a given heater input power.

3. The tank pressure decay potential is significant at high fluid density conditions. When the system is undisturbed, the pressure decay potential becomes progressively higher as a result of rapid successive heater cycles.

4. Satisfactory solutions to the variable fluid property, low-g heat transfer problem, throughout the fluid density range can be obtained through the use of a reference temperature procedure.

5. The semi-empirical approach to the model formulation does yield reasonably accurate predictions of the supercritical cryogenic system behavior and provide data well suited for design applications.

Nomenclature

c_p	Specific heat at constant pressure, Btu/lb-R
d	Diameter of heater, outside, ft
$\mathcal{F}_{w,k}$	Node-to-node interchange factor
g	Acceleration, ft/hr^2
Gr	Grashof Number - $g\beta\Delta Tx^3/\nu^2$
h	Enthalpy, Btu/lb
h_x	Heat transfer coefficient, Btu/hr-sq ft-R
j,k	indices
k	Thermal conductivity, Btu/hr-ft-R
L	Length of equivalent plate, ft
m	Mass, lb
$\dot{m}$	Mass rate, lb/hr
$\dot{m}_o$	Expulsion rate, lb/hr
$\dot{m}_t$	Total mass rate, includes expulsion rate, lb/hr
Nu_x	Nusselt number - $h_x x/k$
p	Pressure, lb/sq ft
Pr	Prandtl number - $c_p\mu/k$
q	Heat flux, Btu/hr-sq ft
Q	Heat, Btu
$\dot{Q}$	Heat rate, Btu/hr
$\dot{Q}_{eb}$	Interfacial heat transfer rate from external to bulk cell, Btu/hr

Nomenclature (Continued)

$\dot{Q}_{hi}$	Heat transfer rate from the heater interior surface to internal cell, Btu/hr
t	Time, hr
T	Temperature, R
T_{ref}	Reference temperature, R
T_w	Wall temperature, R
u	Internal energy, Btu/lb
u	Velocity in the x direction, ft/hr
U	Energy, Btu
v	Velocity in the y direction, ft/hr
V	Volume, cu ft
V_t	Total volume, cu ft
x	Distance in the x direction, ft

Greek

α	Temperature ratio, $(T_w - T_{ref})/(T_w - T_b)$, dimensionless
β	Expansion coefficient, $\frac{1}{\rho}\left(\frac{\partial \rho}{\partial T}\right)_p$, 1/R
Γ	Transfer parameter, $V/[\phi(\rho\psi - p)]$, ft^5/lb
δ	Boundary layer thickness, ft
ϵ	dV/dt, ft^5/lb
η	Energy rate parameter, Btu/hr
θ	Transfer parameter, $-\rho\left(\frac{\partial h}{\partial \rho}\right)_p$, Btu/lb

Nomenclature (Continued)

Greek (Continued)

ν	Kinematic viscosity, ft^2/hr
ρ	Density, lb/cu ft
ρ_{cr}	Density at critical temperature, lb/cu ft
σ	Stefan-Boltzman constant, Btu/hr-sq ft-R^4
ϕ	Transfer parameter, $1/\rho\ (\partial p/\partial u)_\rho$, dimensionless
ψ	Transfer parameter, $\rho(\partial u/\partial \rho)_p$, Btu/lb
Ω	Transfer parameter, $[\eta + (u + \psi)\ \dot{m}]/\ (\rho\psi - p)$, cu ft/hr

Subscripts

b	Bulk
c	Conduction
e	External
i	Internal
k	Inlet
ℓ	Boundary layer
r	Radiation

References

1. Ostrach, S., "An Analysis of Laminar Free-Convection Flow and Heat Transfer About a Flat Plate Parallel to the Direction of the Generating Body Force," NACA TR 1111, (1953).

2. Sparrow, E. M. and Gregg, J. L., "The Variable Fluid-Property Problem in Free Convection," Trans. ASME, 80, 879, (1958).

3. Eckert, E. R. G., and Drake, R. M., "Heat and Mass Transfer," McGraw-Hill, 2nd Edition, (1959).

4. Martini, W. R. and Churchill, S. W., "Natural Convection Inside a Horizontal Cylinder," A.I.Ch.E. Journal, 6, 251, (1960).

5. Weinbaum, S., "Natural Convection in a Horizontal Circular Cylinder," J. of Fluid Mech., 18, (1964).

6. Shaidvrov, G. F., "Convective Heat Transfer in Horizontal Cylinder," Int. J. Heat Mass Transfer, 2, 280, (1960).

7. Weber, L. A., "Thermodynamic and Related Properties of Oxygen from the Triple Point to 300 K at Pressures to 330 Atmospheres Supplement A (British Units)," NBS Report 9710 A, (August 1968).

8. Hess, H. L. and Kunz, H. R., "A Study of Forced Convection Heat Transfer to Supercritical Hydrogen," Trans ASME, 87, 41, (1965).

9. Hendricks, R. C. and Simoneau, R. J., "Survey of Heat Transfer to Near Critical Fluids," NASA TM X-52612, (June 1969).

10. Deissler, R. G., "Heat Transfer and Fluid Friction for Fully Developed Turbulent Flow of Air and Supercritical Water with Variable Fluid Properties," Trans. ASME, 56, 73, (1954).